THE JOURNAL OF PHYSICAL CHEMISTRY C

Article

pubs.acs.org/JPCC

A Theoretical Study of the Effect of Zr-, Nb-Doped and Vacancy-like Defects on H Desorption on MgH_2 (110) Surface

Estefanía Germán,*[,†,‡] Valeria Verdinelli,[‡] Carla R. Luna,[‡] Alfredo Juan,[‡] and David Sholl[†]

[†]School of Chemical and Biomolecular Engineering, Georgia Institute of Technology, Atlanta, Georgia 30332, United States

[‡]Instituto de Física del Sur (IFISUR, UNS-CONICET) and Departamento de Física, Universidad Nacional del Sur, 1253 Alem Avenue, B8000CPB Bahía Blanca, Argentina

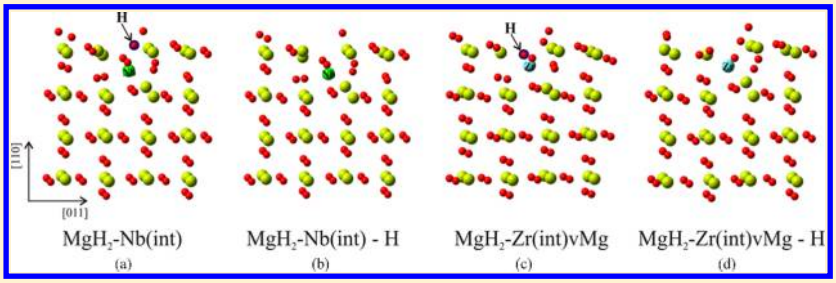

ABSTRACT: DFT calculations were used to study hydrogen desorption energy in a set of pure, Nb- or Zr-doped systems, containing vacancy-like defects and a MgH_2 (110) defect-free surface. The preferential location site for dopants was determined by means of occupation energy analysis. Both transition metal atoms (Nb and Zr) preferred interstitial sites. The effect of vacancies in the systems was also considered. MgH_2 with a Nb interstitial atom and MgH_2 with a Zr interstitial atom containing a Mg vacancy modifies the surface geometry and weakens the Mg−H bonds thus easing the H desorption process.

1. INTRODUCTION

Among metal hydrides, magnesium hydride is one of the most promising candidates as hydrogen storage media in the automotive industry due to its very high capacity (7.6 wt %) and low cost.[1,2] Nevertheless, a slow hydriding and dehydrogenating kinetics and a high dissociation temperature limit its practical application for hydrogen storage. The mechanical alloy of MgH_2 and transition metal (TM) elements have been experimentally proven to be an efficient method. For example, Ni, V, Ti, Fe, Co, and Mn can effectively improve the hydriding and dehydrogenating kinetics of MgH_2 at high temperature (over 573 K).[2−9] The reasons for such behavior are that hydrogen molecules do not readily dissociate on a Mg surface and that magnesium hydride has a high thermodynamic stability.[10,11]

MgH_2 has a high thermodynamic stability that is responsible for the high dehydrogenation temperature requirement of 573 K. Its slow hydrogen sorption kinetics still further restricts the application of MgH_2 for on-board hydrogen storage.[12] The thermodynamics of the dehydrogenation reaction of MgH_2 can also be tuned by doping it with different TM.[2,9,13,14] Recently, Larsson et al.[15] carried out first principles calculations based on DFT to show that Ti, V, Fe, and Ni significantly lowered the H_2 desorption energies of MgH_2 nanoclusters. A computational study carried out by Liang[16] using DFT showed that substitution of two Mg atoms in MgH_2 by a Li and an Al atom may improve its hydrogen storage capability by lowering reaction energies as well as activation barriers. As mentioned before, improvements in its H_2 sorption kinetics have been attributed to catalytic effects of a variety of TM,[2,9] metal oxides and transition metal oxides.[17−19] Li et al.[20] provided a theoretical understanding of the dehydrogenation mechanism in Nb_2O_5 activated MgH_2. Using a combination of density functional theory (DFT)[21] and ab initio molecular dynamics simulations they showed that the substitution of Nb at the Mg site followed by the clustering of H around Nb atoms was a likely pathway for hydrogen desorption. Several experimental[22,23] and theoretical studies[24−26] have shown that the reaction of MgH_2 with amides, complex metal hydrides, and light metals destabilizes it and lowers its dehydrogenation reaction energy.

Despite the many experimental studies of dehydrogenation on a MgH_2 surface, little is known about surface properties and H_2 desorption in MgH_2 system. Theoretically, ab initio DFT calculations have shown significant predictive power for catalysis and could help to design new alloy catalysts. So far, there have been some theoretical calculations to study Mg−H bonding properties, but most of them are mainly limited to cluster calculations[27,28] or bulk calculations using the local density approximation (LDA),[29,30] which may suffer from strong overbinding.[31]

Most research work has been done on the dehydrogenation of MgH_2 in bulk form. However, only a few studies concerned with enhancement in the desorption mechanism from MgH_2 surfaces have been reported in the literature. Doping metals

Received: November 28, 2013
Revised: January 23, 2014
Published: February 5, 2014

   dx.doi.org/10.1021/jp411714d | J. Phys. Chem. C 2014, 118, 4231−4237

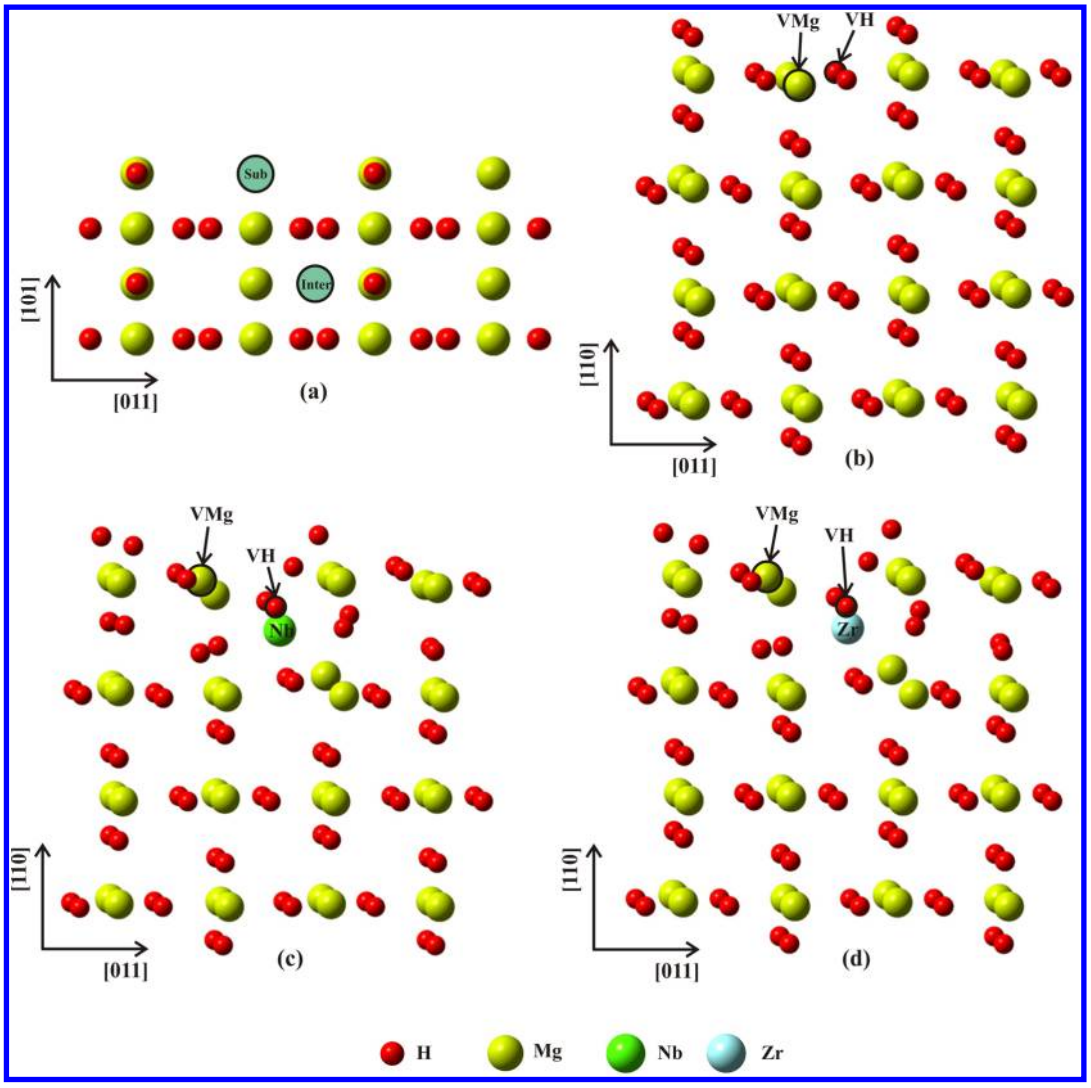

Figure 1. (a) Top view of the supercell. Substitutional and interstitial sites are indicated with green circles, (b) side view of the MgH_2 (110) slab, (c) side view of MgH_2–Nb (Inter), and (d) side view of MgH_2–Zr (Inter). Vacancy generation for dopants and atoms is also shown (vH, vMg, and vMgH).

(light metals or TM) have been used to reduce the stability of MgH_2 surfaces.

Dai et al.[32,33] have employed the DFT in order to thoroughly analyze the hydrogen desorption by doping metals including Al, Ti, Mn, and Ni on MgH_2 (001) and (110) surfaces. The dopant site preference and the desorption mechanism on both surfaces was explored. They reported that each dopant improves the dehydrogenation properties of MgH_2 in a different way. It is still an open question how vacancy-type defects affect the thermodynamics of doping.

In the present work, we have studied the preferential site of Zr and Nb dopants on the MgH_2 (110) surface and we have also considered the effect of vacancy-like defects (Mg, H, or Mg–H complex) in order to improve H desorption energy and to understand dehydrogenation properties and electronic structure. We have also studied the changes in chemical bonding during H desorption using the concept of overlap population (OP).

2. COMPUTATIONAL METHODS AND MODEL

Electronic structure and energy calculations have been carried out within the frame of the DFT[21] as implemented in the Vienna ab initio simulation package (VASP) code.[34,35] The projector augmented wave (PAW) pseudopotential[36,37] was used to account for the electron–ion core interaction, using the PW91 functional as generalized gradient approximation (GGA)[38] for the exchange–correlation term.

MgH_2 surfaces were studied using a (2 × 2) slab containing 32 Mg and 64 H atoms with a 20 Å vacuum in the [110] direction. The Brillouin-zone was sampled using a 7 × 7 × 1 Monkhorst-Pack *k*-point mesh.[39] For the plane-wave basis set a cutoff of 650 eV was used. We checked the influence of strain effects relaxing the first three layers, the first four layers, and carrying out a full relaxation of the system. The total energy difference is lower than 1%, indicating that the influence of strain effects is weak in the bottom layers. To minimize the computational cost we relaxed the first three layers of the slab while the bottom two layers were kept fixed to the bulk positions. The total energy convergence and the forces on the atoms were less than 10^{-4} eV and 0.01 eV/Å, respectively. Self-consistent calculations were considered to converge when the difference in surface total energy between consecutive steps did not exceed 10^{-5} eV. In addition, static calculations were considered to converge using the same criterion. To analyze the

dx.doi.org/10.1021/jp411714d | J. Phys. Chem. C 2014, 118, 4231–4237

electronic structure and bonding we have used the concept of density of states (DOS) and overlap population (OP).[40−44] The OP was calculated using the ADF code.[45] A similar analysis was reported in refs 46 and 47.

In a previous work, we have calculated lattice parameters for the pure perfect MgH_2 cell, which has a rutile type tetragonal structure (P42/mnm, group No. 136), specified by a lattice parameter a and the c/a ratio, a = 4.501 Å, c/a = 6.674, and u = 3.22 Å. These results are in full agreement with experimental values.[48,49] The MgH_2 (110) surface is computed using these bulk parameters. TM dopants are added to the surface considering two different configurations: in the first TM there is a substituent atom replacing a superficial Mg atom (called Sub), and in the second there is a TM located in an interstitial site (called Inter). Figure 1 shows the slab, the location of dopants and the vacancies generated. Occupation energy (E_{occ}) is calculated in order to recognize the preference site of dopants in the surface and the relative stability of the doped system compared to pure MgH_2, using the following definition

$$E_{occ} = E(Mg_{32-x}TM_{x+y}H_{64}) - [E(Mg_{32}H_{64}) + (x + y)E(TM) - xE(Mg)]$$

being (x = 1, y = 0) when TM substitutes a superficial Mg atom and (x = 0, y = 1) when TM is located in an interstitial site.

As mentioned above, hydrogen vacancy (vH), magnesium vacancy (vMg), and complex hydrogen−magnesium vacancy (vMgH) were also considered in the surface. In all cases, the extracted atoms are first neighbors to TM. We also calculated the formation energy of vacancies in all systems

$$E_{vH} = E(Mg_{32-x}TM_{x+y}H_{64-1}) + \frac{1}{2}E(H_2) - E(Mg_{32-x}TM_{x+y}H_{64})$$

$$E_{vMg} = E(Mg_{32-x-1}TM_{x+y}H_{64}) + E(Mg) - E(Mg_{32-x}TM_{x+y}H_{64})$$

$$E_{vMgH} = E(Mg_{32-x-1}TM_{x+y}H_{64-1}) + \frac{1}{2}E(H_2) + E(Mg) - E(Mg_{32-x}TM_{x+y}H_{64})$$

The model used is shown in Figure 1. We can see the MgH_2 cell containing 32 Mg atoms and 64 H atoms, the substitutional and interstitial sites where the TM is located in the unit cell (a), where vacancies are in the pure system (b), and when the Nb and Zr dopants are present (c,d).

3. RESULTS AND DISCUSSIONS

3.1. Geometry and Energy Optimization. Pure-MgH_2 and four different systems (MgH_2-Nb (sub), MgH_2-Nb (inter), MgH_2-Zr (sub), MgH_2-Zr (inter)) were relaxed in order to find the optimum geometry and energy. Table 1 shows computed energies. These results suggest that Zr and Nb atoms prefer to be placed in an interstitial location (1.313 and 1.643 eV, respectively). Dai et al.[33] studied the same surface doped with other TM and found that Ti, Mn, and Ni atoms have an energetic preference for interstitial places as well. When one Nb atom substitutes a Mg atom, the occupation energy becomes more favorable, being the highest among the situations considered (3.023 eV). We can also see in Table 1 that either as substituent or interstitial site, occupancy energy is lower for the Zr dopant compared to the energy for the Nb dopant. Formation energies for vacancies in the case of nondoped MgH_2 are large, especially for the generation of vMg and vMgH (4.890 and 3.694 eV, respectively). However, when these vacancies are created in a doped system, formation energies decrease significantly, in particular in the MgH_2-Nb (sub) system. However, we should not forget that this Nb location has the highest occupation energy, making it less favorable from an energetic point of view. It is necessary to reach a balance between occupation energy and vacancy formation energy. Those systems where a TM is placed in the interstitial site seem to be the most appropriate.

Table 1. Dopant Occupation (E_{occ}) and Vacancy Formation Energies (E_v) in eV for MgH_2 (110) Surface

	E_{occ}	E_{vH}	E_{vMg}	E_{vMgH}
pure-MgH_2		1.587	4.890	3.694
MgH_2-Nb(sub)	3.023	−0.518	0.498	−2.048
MgH_2-Nb(inter)	1.643	0.004	0.234	0.305
MgH_2-Zr(sub)	1.693	0.941	0.707	1.255
MgH_2-Zr(inter)	1.313	1.054	0.014	0.516

3.2. Density of States. As a reference, the total density of states (DOS) of MgH_2 bulk is plotted in Figure 2a. The total and projected (for Mg and H) densities of states of the pure MgH_2 (110) surface are shown in Figure 2 from panel b to panel d. The DOS plot corresponding to MgH_2 bulk shows a band gap of about 4 eV with a large dispersion of the bands signaling the s-like character. An underestimation of the energy gap compared to experimental data is expected for this type of calculations (DFT-GGA).[50] In the case of the MgH_2 (110) surface, this band gap is of approximately 3 eV, that is, 1 eV lower than the gap computed for the bulk. In addition, the sign above the Fermi level is less intense.[32] The Fermi level is placed immediately above the valence band and this band spreads out about −7.5 eV and presents two sharp peaks, one approximately at −1.8 eV and the other at the Fermi level. Analyzing the projected DOS curves we can notice that these correspond to the bonding between Mg and H electrons showing a strong hybridization that is responsible for the high cohesion energy of MgH_2. The conduction band is dominated by Mg s and p states and the valence band mainly by H-s states. In the projected DOS curve for the H atom, the intensity is a result of the weight of H in the structure and also of the transfer of electrons from Mg to H leading to an ionic hydride. The relatively large band gap of MgH_2 leads to a relatively high formation energy of MgH_2 and poor hydrogen sorption kinetics.[51] In the bulk, the interaction between Mg and H atoms is stronger than in the surface where the intensity of the valence band diminishes. These weak bonding interactions between Mg and H in the surface are the reasons why this system is more feasible to react with TM.

Figure 2 also presents the MgH_2-Nb-doped (inter) DOS curves (a−h). The total DOS plot shows a noticeable decrease in the band gap of about 2 eV. A new band appears around −1.5 and −2 eV, although it is the product of H, Mg, and Nb interaction where Nb dopant is the main contributor.

The Zr-doped system is shown in Figure 2i−l. The total DOS plot presents a decrease in the band gap of about 1.4 eV. A new band appears around E_F and −0.6 eV, although it is the product of H, Mg, and Zr interaction, the Zr dopant is the main contributor. The projected DOS curves of Mg and H atoms are

dx.doi.org/10.1021/jp411714d | J. Phys. Chem. C 2014, 118, 4231−4237

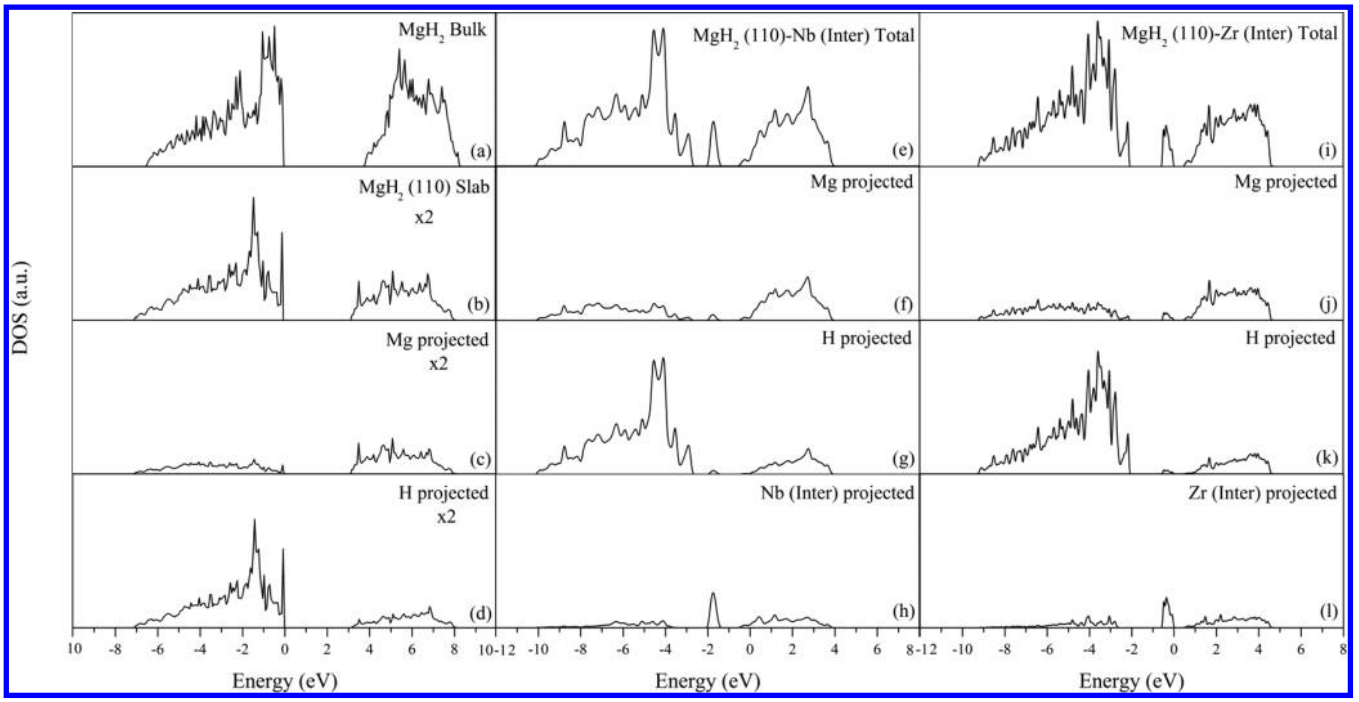

Figure 2. DOS curves corresponding to (a) MgH_2 bulk, (b) MgH_2 (110) slab, (c) Mg atoms projected, and (d) H atoms projected from MgH_2 surface. (e) MgH_2-Nb (inter) total, (f) Mg atoms projected, (g) H atoms projected, and (h) Nb atom projected corresponding to MgH_2-Nb (inter) surface. (i) MgH_2-Zr (inter) total, (j) Mg atoms projected, (k) H atoms projected, and (l) Zr atom projected corresponding to MgH_2-Zr (inter) surface.

reduced at E_F due to the presence of Zr dopant, thus decreasing the Mg−H hybridization. These behaviors can be attributed to a weakening in Mg−H interaction.[52]

Doping leads to the appearance of a narrow d-band in the middle of the band gap. Zr atoms have 2 d electrons and Nb atoms have 4 d electrons, as the d-band fills E_F shifts. Taking into account that these d-states are strongly hybridized with s-states of H atoms giving a strong TM-H bonding and a decrease in the band gaps, we can conclude that Mg−H dissociation will be easier and the H desorption energy will be lower when the MgH_2 (110) surface is doped with Zr and Nb atoms.

3.3. Hydrogen Desorption. The hydrogen desorption energy for the different MgH_2 (110) surface systems was computed according to ref 33

$$E_{des} = E(Mg_{32-x}M_{x+y}H_{64-1}) + \frac{1}{2}E(H_2) - E(Mg_{32-x}M_{x+y}H_{64})$$

where $Mg_{32-x}M_{x+y}H_{64-1}$ is a pseudostructure in which a H atom is removed from the relaxed $Mg_{32-x}M_{x+y}H_{64}$ system. The energy of the hydrogen molecule is computed as −6.773 eV using a 10 × 10 × 10 Å supercell in full agreement with experimental data.[33] Desorption energy values are listed in Table 2 after removing a surface H atom.

The theoretical calculation of MgH_2 dehydrogenation energy in the core of a bulk solid is 1.60 eV while the experimental value is 1.70 eV.[35,53] This energy is lower in the pure MgH_2 (001) surface because those Mg−H bonds are not as strong as in bulk.

The H desorption energy decreases significantly in almost all doped systems, that is, from 1.59 to 0.07, 0.16, and 0.95. In the case of Nb substituting a Mg atom, this energy is −0.61 eV indicating that no energy is required to lose a H atom, thus, this system has the highest occupation energy (see Table 1). After surface relaxation, we found that the substitution of Mg by a Nb atom distorts ionic positions, pushing away two Mg and two H atoms, thus making H desorption easy. This net distortion could be responsible for the high occupation energy. When vacancies are generated in pure MgH_2, H desorption energy decreases −60% in the case of vH. In the case of vMg and vMgH, this energy becomes negative indicating a spontaneous dehydrogenation (−1.20 and −1.90 eV). When a VMg is considered, Mg−H bonds elongate 13% and the geometry after relaxation locates two H atoms moving outside the surface. When both Mg and H vacancies are considered two H atoms diminish their coordination with Mg, that is, H is bonded to only one Mg atom instead of two or three. It should be remembered that the energy needed to create these vacancies is high, that is, from 1.587 to 4.890 eV. When vacancies (vH, VMg, or vMgH) are present in doped systems, the H desorption energy decreases in comparison to the pure MgH_2 (110) without vacancies (except for MgH_2−Nb (sub) vMgH), and this energy increases if we compare it with the no doped

Table 2. Hydrogen Desorption Energy, E_{des} (eV), for TM Doped and Pure MgH_2 (110) Surface with and without Vacancies

	E_{des} (eV)			
		vH	vMg	vMgH
pure-MgH_2	1.59	0.65	−1.20	−1.90
MgH_2-Nb(sub)	−0.61	0.84	−2.55	2.71
MgH_2-Nb(inter)	0.07	1.22	0.07	1.31
MgH_2-Zr(sub)	0.16	0.61	0.55	0.47
MgH_2-Zr(inter)	0.95	0.93	0.50	1.09

dx.doi.org/10.1021/jp411714d | J. Phys. Chem. C 2014, 118, 4231−4237

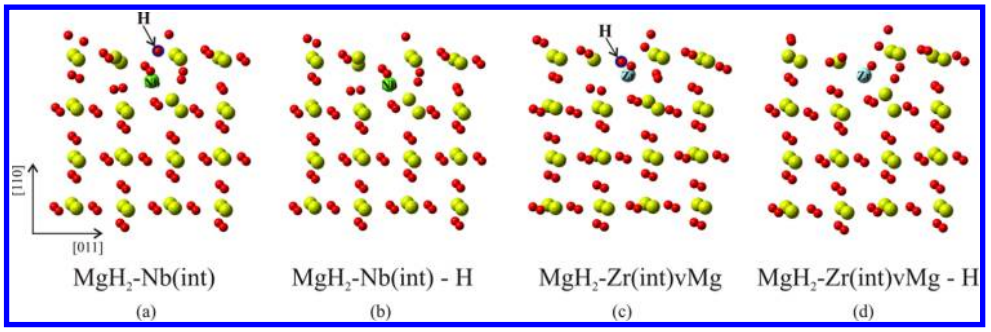

Figure 3. (a) MgH_2-Nb(int), (b) MgH_2-Nb(int)−H, (c) MgH_2-Zr(int)vMg, (d) MgH_2Zr(int)vMg−H atom positions after relaxation. The desorbed H atom is marked with a blue circle.

MgH_2 containing the same type of vacancies, except for MgH_2-Nb (sub) vMg and MgH_2-Zr (sub) vH.

Taking into account the values in Tables 1 and 2 we can conclude that the optimum systems where H desorption is easier are MgH_2-Nb (inter) and MgH_2-Zr (inter) vMg. The relaxed geometry of these two configurations enhances hydrogen desorption, weakening Mg−H bonds (12.5 and 6.5%, respectively) while decreasing the number of H bonds, allowing its extraction with less energy cost. Figure 3 shows the geometries of (a) MgH_2-Nb (inter), (b) MgH_2-Nb (inter)−H, (c) MgH_2-Zr (Inter)vMg, and (d) MgH_2-Zr (Inter)vMg−H systems (before and after H desorption). TM remains almost in the same position after H desorption; however, a displacement of Mg and H atoms occurs in the surface and, the atoms rearrange in the structure with a more stable configuration.

3.4. Bonding Analysis. Table 3 presents the overlap population values for Mg−H and MT−H bonds. When vacancies are generated in the pure MgH_2, the Mg−H bond OP values decrease from 1.67 to 87.85%, making H desorption easier. In the case of MgH_2 containing a Nb atom as a Mg substituent, H desorption energy diminishes significantly as we can see in Table 2. Mg−H bonds weaken in a range of 10.59 to 47.08%, compared to pure MgH_2, while a Nb−H strong bond is developed with an OP value of 0.453. This last interaction also decreases the strength of Mg−H bonds. When a H vacancy is generated, the Mg−H and Nb−H bonds weaken (74.22 and 7.95%, respectively). This is not the case when a Mg vacancy or a complex MgH vacancy is considered on the surface.

We have also considered a Nb atom as an interstitial atom located between the first and second Mg layer. In this case, we found that the Mg−H bonds decrease their OP by 26.67% and 66.67% while a Nb−H bond is formed. The H desorption energy in this system is very low (0.07 eV, see Table 2). When vacancies (vH, vMg, or vMgH) are present, the Mg−H bonds weaken and the MT−H bonds do not suffer significant changes.

In the case of a Zr atom as a Mg substituent, we can notice that Mg−H bonds are a little bit stronger and that a Zr−H bond is formed. When a H vacancy is generated in the system, the Mg−H bonds diminish their strength (24.39 and 1.85%) while the Zr−H bond increases its OP by 7.33%. If a Mg vacancy or a MgH complex vacancy is present in the surface, bonds are stronger and the H desorption energy increases its value, becoming more difficult than the same system without vacancies.

Zr as an interstitial atom in the surface increases the strength of some Mg−H bonds and diminishes the strength of others (+8.75 and −29.91%). At the same time, a Zr−H bond is formed with an OP value of 0.159, the weaker MT−H bond found here. When a H vacancy or a Mg vacancy is considered in the surface, the Mg−H bond also weakens, while the Zr−H bonds do not change significantly. In the case of a MgH complex vacancy, the Mg−H bonds are strengthened.

Table 3. Overlap Population (OP) Values[a]

	MgH_2	MgH_2-vH	MgH_2-vMg	MgH_2-vMgH
Mg−H(1)	0.240	0.236	0.123	0.267
Mg−H(2)	0.321	0.301	0.039	0.285
	MgH_2-Nb(sub)	MgH_2-Nb(sub)vH	MgH_2-Nb(sub)vMg	MgH_2-Nb(sub) vMgH
Mg−H(1)	0.127	0.098	0.170	0.149
Mg−H(2)	0.287	0.074	0.323	0.178
MT-H	0.453	0.417	0.418	0.457
	MgH_2-Nb(int)	MgH_2-Nb(int)vH	MgH_2-Nb(int) vMg	MgH_2-Nb(int) vMgH
Mg−H(1)	0.176	0.145	0.146	0.214
Mg−H(2)	0.107	0.076	0.066	0.051
MT-H	0.429	0.431	0.474	0.423
	MgH_2-Zr(sub)	MgH_2-Zr(sub)vH	MgH_2-Zr(sub) vMg	MgH_2-Zr(sub) vMgH
Mg−H(1)	0.246	0.186	0.318	0.277
Mg−H(2)	0.324	0.318	0.314	0.215
MT-H	0.191	0.205	0.276	0.323
	MgH_2-Zr(int)	MgH_2-Zr(int) vH	MgH_2-Zr(int) vMg	MgH_2-Zr(int) vMgH
Mg−H(1)	0.261	0.222	0.249	0.325
Mg−H(2)	0.225	0.214	0.169	0.225
MT-H	0.159	0.129	0.161	0.138

[a]The number beside each element denotes the layer in which it is placed (see Figure 1).

4. CONCLUSIONS

DFT calculations were carried out in order to compute hydrogen desorption energy in a MgH_2 (110) surface doped with Nb and Zr. We also investigated the effect of vacancy-like defects (Mg, H, or Mg−H complex) in H desorption energy. TM dopants are added to the surface in two different situations, substituent and interstitial sites, both Zr and Nb prefer an interstitial site occupancy. The DOS curves show that the decrease in bond strengths and band gaps lead to an easier Mg−H dissociation and lower H desorption energy when the MgH_2 (110) surface is doped with Zr or Nb. The H desorption

dx.doi.org/10.1021/jp411714d | J. Phys. Chem. C 2014, 118, 4231−4237

energy diminishes its value noticeably in doped systems and the neighboring atoms rearrange their positions making Mg−H bonds even weaker. It is necessary to balance the occupation and H desorption energies in order to conclude which system is best suited for the dehydrogenation process. MgH_2-Nb(int) and MgH_2-Zr(int)vMg systems have the lowest occupation energy and a low H desorption energy (0.07 and 0.50 eV, respectively). Although MgH_2-Nb(sub) has a H desorption energy of −0.61 eV, this system is not appropriate due to its high occupation energy (3.023 eV) in comparison to MgH_2-Nb(int) and MgH_2-Zr(int) systems (1.643 and 1.313 eV, respectively).

AUTHOR INFORMATION

Corresponding Author

*E-mail: egerman@uns.edu.ar.

Notes

The authors declare no competing financial interest.

ACKNOWLEDGMENTS

The authors acknowledge SGCyT (UNS), IFISUR-CONICET, CIC - Buenos Aires, PICT 1770 and PICT-2012-1609 for financial support. E.G., V.V., C.L., and A.J. are members of CONICET. E.G. acknowledges the Fulbright Commission for research fellowship. We thank useful discussions with Dr. Carlos Macchi.

REFERENCES

(1) Schlapbach, L.; Zuttel, A. Hydrogen-Storage Materials for Mobile Applications. *Nature* **2001**, *414*, 353−358.

(2) Liang, G.; Huot, J.; Van Neste, A.; Schulz, R. Catalytic Effect of Transition Metals on Hydrogen Sorption in Nanocrystalline Ball Milled MgH_2−TM (TM=Ti, V, Mn, Fe and Ni) Systems. *J. Alloys Compd.* **1999**, *292*, 247−252.

(3) Song, Y.; Guo, Z. X.; Yang, R. Influence of Selected Alloying Elements on the Stability of Magnesium Dihydride for Hydrogen Storage Applications: A First-Principles Investigation. *Phys. Rev. B* **2004**, *69*, 094205−094215.

(4) Rivoirard, S.; de Rango, P.; Fruchart, D.; Charbonnier, J.; Vempaire, D. Catalytic Effect of Additives on the Hydrogen Absorption Properties of Nano-Crystalline MgH_2(X) Composites. *J. Alloys Compd.* **2003**, *356*−*357*, 622−625.

(5) Shang, C. X.; Bououdina, M.; Song, Y.; Guo, Z. X. Mechanical Alloying and Electronic Simulations of (MgH_2+M) Systems (M=Al, Ti, Fe, Ni, Cu and Nb) for Hydrogen Storage. *Int. J. Hydrogen Energy* **2004**, *29*, 73−80.

(6) Liang, G.; Huot, J.; Boily, S.; Schulz, R. Hydrogen Desorption Kinetics of a Mechanically Milled MgH_2+5 atom %V Nanocomposite. *J. Alloys Compd.* **2009**, *305*, 239−245.

(7) Arico, A. S.; Bruce, P.; Scrosati, B.; Tarascon, J. M.; Van Schalkwijk, W. Nanostructured Materials for Advanced Energy Conversion and Storage Devices. *Nat. Mater.* **2005**, *4*, 366−377.

(8) Tsuda, M.; Dino, W. A.; Kasai, H.; Nakanishi, H. Magnetized/Charged MgH_2-Based Hydrogen Storage Materials. *Appl. Phys. Lett.* **2005**, *86*, 213109-1−213109-3.

(9) Hanada, N.; Ichikawa, T.; Fujii, H. Catalytic Effect of Nanoparticle 3d-Transition Metals on Hydrogen Storage Properties in Magnesium Hydride MgH_2 Prepared by Mechanical Milling. *J. Phys. Chem. B* **2005**, *109*, 7188−7194.

(10) Zaluska, A.; Zaluski, L.; Strom-Olsen, J. O. Structure, Catalysis and Atomic Reactions on the Nano-Scale: a Systematic Approach to Metal Hydrides for Hydrogen Storage. *Appl. Phys. A* **2001**, *72*, 157−165.

(11) Von Zeppelin, F.; Reule, H.; Hirscher, M. Hydrogen Desorption Kinetics of Nanostructured MgH_2 Composite Materials. *J. Alloys Compd.* **2002**, *330*−*332*, 723−726.

(12) Bogdanovic, B.; Hartwig, H. T.; Spliethoff, B. The Development, Testing and Optimization of Energy Storage Materials Based on the MgH_2-Mg System. *Int. J. Hydrogen Energy* **1993**, *18*, 575−589.

(13) Song, Y.; Guo, Z. X.; Yang, R. Influence of Titanium on the Hydrogen Storage Characteristics of Magnesium Hydride: a First Principles Investigation. *Mat. Sc. & Eng. A* **2004**, *365*, 73−79.

(14) Song, Y.; Guo, Z. X.; Yang, R. Influence of Selected Alloying Elements on the Stability of Magnesium Dihydride for Hydrogen Storage Applications: A First-Principles Investigation. *Phys. Rev. B* **2004**, *69*, 094205−1−094205−11.

(15) Larsson, P.; Araujo, C. M.; Larsson, J. A.; Jena, P.; Ahuja, R. Role of Catalysts in Dehydrogenation of MgH_2 Nanoclusters. *Proc. Natl. Acad. Sci. U.S.A.* **2008**, *105*, 8227−8231.

(16) Liang, J.-j. LiAl-Substitution into the MgH_2 Structure May Improve the Hydrogen Storage Processes. *J. Alloys Compd.* **2007**, *446*−*447*, 72−79.

(17) Song, M. Y.; Bobet, J.-L.; Darriet, B. Improvement in Hydrogen Sorption Properties of Mg by Reactive Mechanical Grinding with Cr_2O_3, Al_2O_3 and CeO_2. *J. Alloys Compd.* **2002**, *340*, 256−262.

(18) Barkhordarian, G.; Klassen, T.; Bormann, R. Fast Hydrogen Sorption Kinetics of Nanocrystalline Mg Using Nb_2O_5 as Catalyst. *Scr. Mater.* **2003**, *49*, 213−217.

(19) Polanski, M.; Bystrzycki, J.; Plocinski, T. The Effect of Milling Conditions on Microstructure and Hydrogen Absorption/Desorption Properties of Magnesium Hydride (MgH_2) without and with Cr_2O_3 Nanoparticles. *Int. J. Hydrogen Energy* **2008**, *33*, 1859−1867.

(20) Li, S.; Jena, P.; Ahuja, R. Dehydrogenation Mechanism in Catalyst-Activated MgH_2. *Phys. Rev. B* **2006**, *74*, 132106−1−132106−4.

(21) Kohn, W.; Sham, L. J. Self-Consistent Equations Including Exchange and Correlation Effects. *Phys. Rev.* **1965**, *140*, A1133−A1138.

(22) Luo, W. ($LiNH_2$−MgH_2): A Viable Hydrogen Storage System. *J. Alloys Compd.* **2004**, *381*, 284−287.

(23) Johnson, S. R.; Anderson, P. A.; Edwards, P. P.; Gameson, I.; Predergast, J. W.; Al-Mamouri, M.; Book, D.; Harris, I. R.; Speight, J. D.; Walton, A. Chemical Activation of MgH_2; a New Route to Superior Hydrogen Storage Materials. *Chem. Commun.* **2005**, *22*, 2823−2825.

(24) Alapati, S. V.; Johnson, J. K.; Sholl, D. S. Predicting Reaction Equilibria for Destabilized Metal Hydride Decomposition Reactions for Reversible Hydrogen Storage. *J. Phys. Chem. C* **2007**, *111*, 1584−1591.

(25) Alapati, S. V.; Johnson, J. K.; Sholl, D. S. Using First Principles Calculations to Identify New Destabilized Metal Hydride Reactions for Reversible Hydrogen Storage. *Phys. Chem. Chem. Phys.* **2007**, *9*, 1438−1452.

(26) Alapati, S. V.; Johnson, J. K.; Sholl, D. S. Identification of Destabilized Metal Hydrides for Hydrogen Storage Using First Principles Calculations. *J. Phys. Chem. B* **2006**, *110*, 8769−8776.

(27) Tsuda, M.; Dino, W. A.; Nakanishi, H.; Kasai, H. Ab Initio Study of H_2 Desorption from Magnesium Hydride MgH_2 Cluster. *J. Phys. Soc. Jpn.* **2004**, *73*, 2628−2630.

(28) Orgaz, E.; Hernandez-Trujillo, J. Chemical Bonding in Ternary Magnesium Hydrides. *Int. J. Quantum Chem.* **2003**, *94*, 150−164.

(29) Yu, R.; Lam, P. K. Electronic and Structural Properties of MgH_2. *Phys. Rev. B* **1988**, *37*, 8730−8737.

(30) Schimmel, H. G.; Johnson, M. R.; Kearley, G. J.; Ramirez-Cuesta, A. J.; Huot, J.; Mulder, F. M. Structural Information on Ball Milled Magnesium Hydride from Vibrational Spectroscopy and Ab-Initio Calculations. *J. Alloys Compd.* **2005**, *393*, 1−4.

(31) Kurth, S.; Perdew, J. P.; Blaha, P. Molecular and Solid-State Tests of Density Functional Approximations: LSD, GGAs, and Meta-GGAs. *Int. J. Quantum Chem.* **1999**, *75*, 889−909.

(32) Dai, J. H.; Song, Y.; Yang, R. Intrinsic Mechanisms on Enhancement of Hydrogen Desorption from MgH_2 by (001) Surface Doping. *Int. J. Hydrogen Energy* **2011**, *36*, 12939−12949.

(33) Dai, J. H.; Song, Y.; Yang, R. First Principles Study on Hydrogen Desorption from a Metal (=Al, Ti, Mn, Ni) Doped MgH_2 (110) Surface. *J. Phys. Chem. C* **2010**, *114*, 11328−11334.
(34) Kresse, G.; Hafner. Ab Initio Molecular-Dynamics Simulation of the Liquid-Metal−Amorphous-Semiconductor Transition in Germanium. *J. Phys. Rev. B* **1994**, *49*, 14251−14269.
(35) Kresse, G.; Hafner. Ab Initio Molecular Dynamics for Liquid Metals. *J. Phys. Rev. B* **1993**, *47*, 558−561.
(36) Kresse, G.; Joubert, D. From Ultrasoft Pseudopotentials to the Projector Augmented-Wave Method. *Phys. Rev. B* **1999**, *59*, 1758−1775.
(37) Blöchl, P. E. Projector Augmented-Wave Method. *Phys. Rev. B* **1994**, *50*, 17953−17979.
(38) Perdew, J. P.; Wang, Y. Accurate and Simple Analytic Representation of the Electron-Gas Correlation Energy. *Phys. Rev. B* **1992**, *45*, 13244−13249.
(39) Monkhorst, H. J.; Pack, J. D. Special Points for Brillouin-Zone Integrations. *Phys. Rev. B* **1976**, *13*, 5188−5192.
(40) Baerends, E. J.; Ellis, D. E.; Ros, P. Self-Consistent Molecular Hartree-Fock-Slater Calculations I. The Computational Procedure. *Chem. Phys.* **1973**, *2*, 41−51.
(41) te Velde, G.; Baerends, E. J. Numerical Integration for Polyatomic Systems. *J. Comput. Phys.* **1992**, *99*, 84−98.
(42) Fonseca Guerra, C.; Visser, O.; Snijders, J. G.; te Velde, G.; Baerends, E. J. *Methods and Techniques in Computational Chemistry*; STEF: Cagliari, Italy, 1995; Vol. *95*, p 305−395.
(43) Hohenberg, P.; Kohn, W. Inhomogeneous Electron Gas. *Phys. Rev.* **1964**, *136*, B864−B871.
(44) Hoffmann, R. *Solids and Surfaces: A Chemist's View of Bonding in Extended Structures*; VCH: New York, 1988.
(45) ADF 2.2.1. *Theoretical Chemistry*; Vrije Universiteit: Amsterdam, 1997.
(46) Luna, C. R.; Macchi, C. E.; Juan, A.; Somoza, A. Electronic and Bonding Properties of MgH_2−Nb Containing Vacancies. *Int. J. Hydrogen Energy* **2010**, *35*, 12421−12427.
(47) López-Corral, I.; Germán, E.; Juan, A.; Volpe, M. A.; Brizuela, G. P. Hydrogen Adsorption on Palladium Dimer Decorated Graphene: A bonding Study. *Int. J. Hydrogen Energy* **2012**, *37*, 6653−6665.
(48) Luna, C. R.; Germán, E.; Macchi, C.; Juan, A.; Somoza, A. On the Perfect MgH_2(−Nb,−Zr) Systems and the Influence of Vacancy-Like Defects on their Structural Properties. A Self-Consistent First Principle Calculations Study of the Electron and Positron Parameters. *J. Alloys Compd.* **2013**, *556*, 188−197.
(49) Bortz, M.; Bertheville, B.; Böttger, G.; Yvon, K. Structure of the High Pressure Phase γ-MgH_2 by Neutron Powder Diffraction. *J. Alloys Compd.* **1999**, *287*, L4−L6.
(50) Yu, R.; Lam, P. K. Electronic and Structural Properties of MgH_2. *Phys. Rev. B* **1988**, *37*, 8730−8737.
(51) Zeng, X. Q.; Cheng, L. F.; Zou, J. X.; Ding, W. J.; Tian, H. Y.; Buckley, C. Influence of 3d Transition Metals on the Stability and Electronic Structure of MgH_2. *J. Appl. Phys.* **2012**, *111*, 093720−093729.
(52) Shelyapina, M. G.; Fruchart, D. Role of Transition Elements in Stability of Magnesium Hydride: A Review of Theoretical Studies. *Diffus. Defect Data, Pt. B* **2011**, *170*, 227−231.
(53) Fernandez, J. F.; Sanchez, C. R. Simultaneous TDS-DSC Measurements in Magnesium Hydride. *J. Alloys Compd.* **2003**, *356*−*357*, 348−352.